

# Magnetic Properties of Quantized Vortices in Neutron ${}^3P_2$ Superfluids in Neutron Stars

Kota Masuda<sup>1,2</sup> and Muneto Nitta<sup>3\*</sup>

<sup>1</sup>*Department of Physics, The University of Tokyo, Tokyo 113-0033, Japan*

<sup>2</sup>*Theoretical Research Division, Nishina Center, RIKEN, Wako 351-0198, Japan*

<sup>3</sup>*Department of Physics at Hiyoshi, and Research and Education Center for Natural Sciences, Keio University, Hiyoshi 4-1-1, Yokohama, Kanagawa 223-8521, Japan*

(Dated: December 8, 2015)

We discuss quantized vortices in neutron  ${}^3P_2$  superfluids, which are believed to realize in high density neutron matter such as neutron stars. By using the Ginzburg-Landau free energy for  ${}^3P_2$  superfluids, we determine the ground state in the absence and presence of the external magnetic field, and numerically construct  ${}^3P_2$  quantized vortices in the absence and presence of the external magnetic field along the vortex axis (poloidal) or angular direction (toroidal). We find in certain situations the spontaneous magnetization of the vortex core, whose typical magnitude is about  $10^{7-8}$  Gauss, but the net magnetic field in a neutron star is negligible because of the ratio of the vortex core size  $\sim 10\text{fm}$  and the intervortex distance  $\sim 10^{-6}\text{m}$  in a vortex lattice.

## I. INTRODUCTION

Neutron stars provide unique laboratories in universe not only for astrophysics but also for nuclear physics and condensed matter physics. Neutron stars have some observables such as the mass ( $M$ ), radius ( $R$ ), surface temperature ( $T_s$ ) and magnetic fields on the surface ( $B_s$ ). The observed masses of neutron stars give a stringent constraint on the stiffness of the equation of state. Other observables such as  $T_s$  and  $B_s$  give us rich information about the states of high density nuclear matter.

It is generally believed that a neutron superfluid state is realized inside neutron stars, which is a high density fermionic system. At low densities less than the normal nuclear matter density, the dominant effective pair interaction is the  ${}^1S_0$  attractive one, and the possibility of  ${}^1S_0$  superfluidity was pointed out by Migdal in 1959 [1]. From the observational point of view, pulsar glitches, which are the sudden speed-up events of neutron stars [2], might show the existence of the superfluidity inside neutron stars, although the mechanism of pulsar glitches is still controversial. The origin of pulsar glitches was proposed to be the starquake from the core or the crust of neutron stars [3–5]. It was also proposed that pulsar glitches can be explained by the unpinning dynamics of a large number of neutron vortices pinned on the nuclei [6]. In spite of several different proposals, there is a common point for the existence of superfluids among several models; The observed long relaxation time  $\tau$  ( $\sim$  weeks for Crab and  $\sim$  years for Vela) can be explained by assuming that neutron stars have the two components, normal neutrons and superfluid neutrons [3–5]. Moreover, recent observation of the cooling process of a neutron star may indicate the existence of superfluid components in the neutron star [7, 8]. Therefore, it is very important to study the detailed properties of neutron superfluidity to understand the dynamics and evolution of neutron stars.

Once it is established, a large number of quantized vortices are inevitably created along the rotation axis due to the rapid rotation of neutron stars, and consequently understanding the dynamics of superfluid vortices should be crucial.

Due to the repulsive core in the  ${}^1S_0$  partial wave, the effects of pairing in the  ${}^3P_2$  attractive interaction becomes comparable to that of the  ${}^1S_0$  case at about the normal nuclear matter density. Therefore, a transition from an isotropic  ${}^1S_0$  superfluid to an anisotropic  ${}^3P_2$  superfluid has been predicted to occur at this density [9–14]. The Ginzburg-Landau (GL) free for the  ${}^3P_2$  superfluid, which is valid near the critical temperature, was derived in Refs. [13, 14] in the weak coupling limit. The ground state was determined in the GL theory to be in the nematic phase [15] according to the classification by Mermin [16] for the GL free energy with total angular momentum two. The strong coupling effect was taken into account in Ref. [17]. Although no definite observational signal of the existence of  ${}^3P_2$  superfluids was obtained yet, the existence of quantized vortices is inevitable if it is realized. Vortex structures in  ${}^3P_2$  superfluids were discussed in the GL equation for the  ${}^3P_2$  superfluid [14, 18, 19]. In particular, the spontaneous magnetization of a vortex was pointed out in Ref. [19]. Recent study of  ${}^3P_2$  superfluids includes for instance low energy excitations, their low energy theory, neutrino emission [20–29], their effects on cooling process [30, 31] and the entrainment [32].

In this paper, we determine the ground state in the presence of magnetic fields, and work out quantized vortex structures in the  ${}^3P_2$  superfluids in the presence and absence of magnetic fields in the framework of the GL theory. Due to the tensorial nature of the order parameter of the  ${}^3P_2$  superfluids, physics depends on the basis in which the tensor order parameter take a form. The vortex was studied before in the absence of the external magnetic field and the sixth order term in the GL free energy, in which case the coordinate basis of the tensor order parameter is cylindrical for the vortex solution with the least energy [14, 18, 19]. We obtain the full

---

\* masuda(at)nt.phys.s.u-tokyo.ac.jp, nitta(at)phys-h.keio.ac.jp

numerical solution in this case. We further take into account the effect of the sixth order term in the absence and presence of the magnetic field. We find that the Cartesian ( $xyz$ ) basis for the tensor order parameter give the least energy configurations in the presence of the sixth order term and/or the magnetic field along the vortex axis while the cylindrical basis are preferred only in the absence of the external magnetic fields or in the presence of the magnetic field along the angular direction encircling the vortex. We construct the vortex profiles in all these cases. We further calculate the magnetization of the vortex core induced by the neutron anomalous magnetic moment and find that it is present only when off-diagonal elements in the tensor order parameter appear around the vortex core; the case that the off-diagonal elements have the same winding number with the diagonal elements when the cylindrical basis is preferred for the tensor order parameter, and the case that the off-diagonal elements have a winding number differed from that of the diagonal elements by two when the Cartesian basis is preferred for the tensor order parameter. Among these, a net magnetization is present for the former case, that is, the case that the sixth order term is negligible in the absence of the magnetic field and the case in the presence of the magnetic fields in the angular direction. For the Cartesian basis, we find a magnetization upward and downward along the vortex axis locally existing in the angular coordinate, with zero net magnetization. In these cases, the typical magnitude of the magnetic field inside the vortex core is about  $10^{7-8}$  Gauss, and the average value is much less when averaged in the vortex lattice.

This paper is organized as follows. In Sec. II we introduce the GL equation for  $^3P_2$  superfluid states and determine the ground states in the absence and presence of the magnetic fields. In the weak coupling limit, degenerate ground states can be parameterized by one parameter. We also point out some analogy to that of  $^3\text{He}$  superfluids and spin-2 Bose-Einstein condensates (BEC). In Sec. III we construct vortex solutions numerically by using the  $^3P_2$  GL equation in various cases in the presence and absence of magnetic fields along the vortex axis or angular direction. In Sec. IV, we calculate a spontaneous magnetization caused by the  $^3P_2$  vortices. Sec. V is devoted to a summary and discussion. In Appendix A we give the detailed calculation to determine the ground states with taking into account the sixth order term. In Appendix B we give full equations of motion of  $^3P_2$  superfluids.

## II. GINZBURG LANDAU FREE ENERGY FOR $^3P_2$ SUPERFLUIDS

In this section, we first give the GL free energy and determine the ground states in various cases in the absence and presence of the magnetic fields.

### II.1. Ginzburg-Landau free energy

The GL free energy for the  $^3P_2$  superfluidity in the weak coupling limit was derived in Refs. [13, 14, 33] assuming the contact interaction. Here let us follow their derivation. To this end, we consider properties of dense neutron matter by the following Hamiltonian  $H$ , which includes a zero range  $^3P_2$  force

$$H = \int d^3\rho \psi^\dagger \left( -\frac{\nabla^2}{2M} - \mu \right) \psi - \frac{1}{2} g T_{\alpha\beta}^\dagger(\rho) T_{\alpha\beta}(\rho) \quad (1)$$

where  $\rho$  denote space coordinates,  $\psi$  is a neutron field,  $\mu$  is a baryon chemical potential,  $M$  is the mass of neutrons, and  $g(>0)$  is the coupling constant. Here,  $\alpha, \beta$  are the space indices, and the tensor  $T_{\alpha\beta}$  is given by

$$T_{\alpha\beta}^\dagger(\rho) = \psi_{\sigma'}^\dagger(\rho) (t_{\alpha\beta}^*)_{\sigma\sigma'}(\nabla) \psi_{\sigma}^\dagger(\rho) \quad (2)$$

with a differential operator  $t$  defined by

$$(t_{\alpha\beta})_{\sigma\sigma'}(\nabla) = \frac{1}{2} ((S_\alpha)_{\sigma\sigma'} \nabla_\beta + \nabla_\alpha (S_\beta)_{\sigma\sigma'}) - \frac{1}{3} \delta_{\alpha\beta} (\mathbf{S})_{\sigma\sigma'} \cdot \nabla \quad (3)$$

and  $\mathbf{S}$  defined by  $(S_\alpha)_{\sigma\sigma'} = i(\sigma_y \sigma_\alpha)_{\sigma\sigma'}$  ( $\alpha = x, y, z$ ).

The order parameter for  $^3P_2$  superfluidity is  $3 \times 3$  traceless symmetric tensor  $A_{\mu i}$ , which is defined by

$$\Delta = \sum_{\mu i} i \sigma_\mu \sigma_y A_{\mu i} k_i \quad (4)$$

where  $\Delta$  is the gap parameter. The Latin letter  $\mu$  stands for the spin index as before while the Roman index  $i$  stands for the spatial coordinates. The symmetry acts on the tensor  $A_{\mu i}$  as

$$A \rightarrow e^{i\theta} g A g^T, \quad e^{i\theta} \in U(1), \quad g \in SO(3) \quad (5)$$

in the matrix notation. The free energy density  $F$  as a function of tensor  $A_{\mu i}$  can be written as

$$F = \int d^3\rho (f_{\text{grad}} + f_{2+4} + f_6 + f_H) \quad (6)$$

where  $f_{\text{grad}}$  is the gradient term,  $f_{2+4}$  and  $f_6$  [33] are the free energy densities up to fourth order and of the sixth order, respectively, and  $f_H$  is the magnetic term, given by

$$f_{\text{grad}} = K_1 \partial_i A_{\mu j} \partial_i A_{\mu j}^\dagger + K_2 (\partial_i A_{\mu i} \partial_j A_{\mu j}^\dagger + \partial_i A_{\mu j} \partial_j A_{\mu i}^\dagger) \quad (7)$$

$$f_{2+4} = \alpha \text{Tr} A A^\dagger + \beta [(\text{Tr} A A^\dagger)^2 - \text{Tr} A^2 A^{\dagger 2}], \quad (8)$$

$$\begin{aligned} f_6 = & \gamma [-3(\text{Tr} A A^\dagger) |\text{Tr} A A^\dagger|^2 + 4(\text{Tr} A A^\dagger)^3 \\ & + 12(\text{Tr} A A^\dagger) \text{Tr} (A A^\dagger)^2 + 6(\text{Tr} A A^\dagger) \text{Tr} (A^2 A^{\dagger 2}) \\ & + 8\text{Tr} (A A^\dagger)^3 + 12\text{Tr} [(A A^\dagger)^2 A^\dagger A] \\ & - 12\text{Tr} [A A^\dagger A^\dagger A^\dagger A A] - 12\text{Tr} A A (\text{Tr} A A^\dagger A A)^*] \end{aligned} \quad (9)$$

and

$$f_H = g'_H H^2 \text{Tr} (A A^\dagger) + g_H H_\mu (A A^\dagger)_{\mu\nu} H_\nu. \quad (10)$$

In Table I, we summarize the coefficients (the GL parameters) calculated in the weak coupling limit by considering only the excitations around the Fermi surface [13, 14, 33]. In this limit,  $K_1$  and  $K_2$  take the same value. In the derivation above, it should be noted that the following relations hold

$$\begin{aligned}\text{Tr}(AA^\dagger(AA^\dagger)^*) &= \text{Tr}(AA^T(AA^T)^*), \\ \text{Tr}((AA^\dagger)^2(AA^\dagger)^*) &= \text{Tr}((AA^\dagger)(AA^T)(AA^T)^*) \\ \text{Tr}(AA^T)\text{Tr}(AA^\dagger AA^T)^* &= \text{Tr}(AA^T)^*\text{Tr}(AA^\dagger AA^T)\end{aligned}$$

because  $A_{\mu i}$  is a symmetric tensor.

We ignore the first term with the coefficient  $g'_H$  of  $f_H$  in Eq. (10) since the effect of this term can be incorporated into the shift of  $\alpha$  in  $f_{2+4}$  and consequently the phase structure is not modified.

Let us make comments on other systems similar to  $^3P_2$  superfluids;  $^3\text{He}$  superfluids and ultracold atomic gases of spin-2 BEC. The  $^3\text{He}$  superfluids are also described by a  $3 \times 3$  tensor  $A_{\mu i}$  but it is not traceless symmetric unlike  $^3P_2$  superfluids [34, 35]. The gradient terms are the same in the weak coupling limit. Spin-2 BECs are described by Gross-Pitaevskii equation of a  $3 \times 3$  traceless symmetric tensor [36]. The sixth order term  $f_6$  is absent in the energy functional of the Gross-Pitaevskii equation. In addition, the terms proportional to  $K_2$  in the gradient term  $f_{\text{grad}}$  are absent in spin-2 BECs. In other words, the terms proportional to  $K_2$  in the gradient term exhibits characteristic features of the  $^3P_2$  superfluids.

## II.2. Ground states

The ground states of the GL free energy with total angular momentum two were classified by Mermin [16]. According to this classification, the ground state of  $^3P_2$  superfluids in the weak coupling limit is in the nematic phase [15].

We summarize the effects of each term on the symmetry breaking pattern in the cases (1)  $f_{2+4}$ , (2)  $f_{2+4} + f_6$ , (3)  $f_{2+4} + f_H$ , and (4)  $f_{2+4} + f_6 + f_H$ .

(1) First, we consider the simplest case  $f_{2+4}$ . The magnitude of the sixth order term is much smaller than that of the fourth order term in the region that the GL theory is appropriate, that is, when the gap parameter is small enough. Here we consider the energy scale in which  $f_6$  is negligible.

At the fourth order level, the ground state  $A_{4\text{th}}$  can be written as

$$A_{4\text{th}}^{(x,y,z)} = \sqrt{\frac{|\alpha|}{\beta(r^2 + (1+r)^2 + 1)}} \begin{pmatrix} r & 0 & 0 \\ 0 & -(1+r) & 0 \\ 0 & 0 & 1 \end{pmatrix} \quad (11)$$

with a continuous degeneracy  $r$  up to the  $SO(3)$  action, where  $(x, y, z)$  implies that we take the Cartesian  $xyz$  coordinates for the indices of the tensor  $A$ . Here,  $r \in \mathbb{R}$  is a parameter whose range can be restricted to  $-1 \leq$

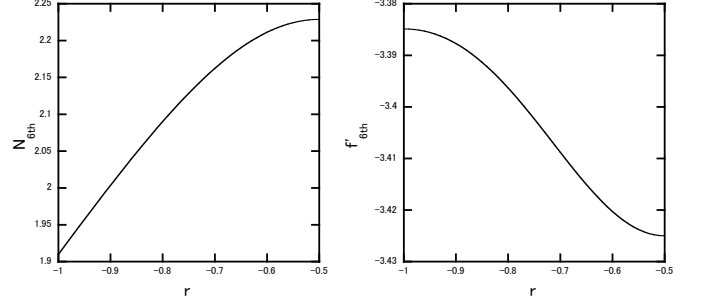


FIG. 1. The normalization and free energy  $f_{2+4} + f_6$ . Left panel: the normalization  $N_{6\text{th}}$  as a function of  $r$ . Right panel:  $f'_{6\text{th}}$  defined by  $f_{2+4} + f_6 \equiv \frac{|\alpha|^2}{6\beta} f'_{6\text{th}}$  as a function of  $r$ . The UN state with  $r = -1/2$  is the ground state.

$r \leq -1/2$  without the loss of generality. In this range, the eigenvalues in the order parameter have the following magnitude relation

$$(1+r)^2 \leq r^2 \leq 1. \quad (12)$$

The ground states are continuously degenerate with parameterized by  $r$  [37] and are referred as the nematic phase. The ground state manifold can be decomposed into three region called strata that have the isomorphic unbroken symmetries  $H$ ; the uniaxial nematic (UN) phase for  $r = -1/2$ ,  $D_2$  biaxial nematic ( $D_2$  BN) phase for  $-1 < r < -1/2$ , and  $D_4$  biaxial nematic ( $D_4$  BN) phase for  $r = -1$ . We summarize the unbroken symmetry  $H$ , the order parameter manifold  $G/H$  and the homotopy groups from  $\pi_0$  to  $\pi_4$  of the order parameter manifold in Table II.

While the order parameter  $G/H$  represent for gapless Nambu-Goldstone (NG) modes, the parameter  $r$  here represents for an additional gapless mode called a quasi-NG mode, that was found in a spin-2 BEC [38]. In the nematic phase, the  $SO(3)$  is enhanced to  $SO(5)$  in the level of the equation of motion, and when it is spontaneously broken, there appears the additional gapless mode, that is, the quasi-NG mode. The whole ground state manifold (extended order parameter manifold) that contains both the NG and quasi-NG modes is  $\frac{U(1) \times SO(5)}{\mathbb{Z}_2 \ltimes SO(4)} \simeq \frac{U(1) \times S^4}{\mathbb{Z}_2}$ .

(2) Next, let us add the sixth order term  $f_6$  (so that the total free energy is  $f_{2+4} + f_6$ ), and see which state is selected by this term. In Appendix A, we show that the ground state is still in the nematic phase in the presence of the sixth order term, with correcting the amplitude of the condensates in the previous study [15]. We can derive the ground state  $A_{6\text{th}}$  exactly by minimizing free energy with the Ansatz,

$$A_{6\text{th}}^{(x,y,z)} = \sqrt{\frac{|\alpha|}{6\beta}} N_{6\text{th}} \begin{pmatrix} r & 0 & 0 \\ 0 & -(1+r) & 0 \\ 0 & 0 & 1 \end{pmatrix}. \quad (13)$$

$\alpha$	$K_1 = K_2$	$\beta$	$\gamma$	$g_H$
$\frac{N(0)}{3} \frac{T - T_c}{T} k_F^2$	$\frac{7\zeta(3)}{240M^2} \frac{N(0)}{(\pi T_c)^2} k_F^4$	$\frac{7\zeta(3)}{60} \frac{N(0)}{(\pi T_c)^2} k_F^4$	$-\frac{31}{16} \frac{\zeta(5)}{840} \frac{N(0)}{(\pi T_c)^4} k_F^6$	$\frac{7\zeta(3)}{24} \frac{N(0)}{(\pi T_c)^2} \frac{(\gamma_n \hbar)^2}{2(1+F)^2} H^2 k_F^2$

TABLE I. The GL parameters in the weak coupling limit. In the derivation of  $\alpha$ , we took  $g = \frac{3\pi^2}{Mk_F^3}$  in order for the  $T$  dependence of  $\alpha$  to become the same with that of the BCS theory. Here,  $k_F$  is the Fermi momentum defined by  $k_F = \hbar c(3\pi^2\rho)^{1/3}$  where  $\rho$  is the neutron density.  $N(0) \equiv \frac{Mk_F}{2\pi^2}$  is the density of states  $N = \frac{Mk}{2\pi^2}$  on the Fermi surface  $k = k_F$ ,  $T_c$  is the critical temperature for the  $^3P_2$  superfluidity and the Riemann zeta function  $\zeta(n)$  is defined by  $\zeta(n) = \sum_{k=1}^{\infty} \frac{1}{k^n}$ , for which  $\zeta(3) \sim 1.202$  and  $\zeta(5) \sim 1.037$ .  $\gamma_n$  is the gyromagnetic ratio of the neutrons and  $F$  is the Fermi liquid correction about the Pauli spin susceptibility. In this paper, we take  $F = -0.75$ ,  $T_c = 0.2\text{MeV}$ ,  $T = 0.8T_c$  and  $\rho = 0.17/\text{fm}^3$  for numerical simulations.

$r$	Phase	$H$	$G/H$	$\pi_0$	$\pi_1$	$\pi_2$	$\pi_3$	$\pi_4$	Physical situation
$-1/2$	UN	$O(2)$	$U(1) \times [SO(3)/O(2)]$	0	$\mathbb{Z} \oplus \mathbb{Z}_2$	$\mathbb{Z}$	$\mathbb{Z}$	$\mathbb{Z}_2$	$f_{2+4} + f_6$
$-1 < r < -1/2$	$D_2$ BN	$D_2$	$U(1) \times [SO(3)/D_2]$	0	$\mathbb{Z} \oplus \mathbb{Q}$	0	$\mathbb{Z}$	$\mathbb{Z}_2$	$f_{2+4} + f_6 + f_H$
$-1$	$D_4$ BN	$D_4$	$[U(1) \times SO(3)]/D_4$	0	$\mathbb{Z} \times_h D_4^*$	0	$\mathbb{Z}$	$\mathbb{Z}_2$	$f_{2+4} + f_H$

TABLE II. The strata in the nematic phase. We show the range of  $r$ , the phase, the unbroken symmetry  $H$ , the order parameter manifold  $G/H$ , the homotopy groups from  $\pi_0$  to  $\pi_4$ , and the physical situations (free energy) that realize these states. \* indicates the universal covering group, and  $\mathbb{Q} = D_2^*$  is a quaternion group. For the definition of the product  $\times_h$ , see §4.2.2 and Appendix A of Ref. [39].

By minimizing the free energy density

$$\begin{aligned}
f_{2+4} + f_6 &= 2\alpha(1 + r + r^2)N_{6\text{th}}^2 \\
&+ \beta(2r^4 + 4r^3 + 6r^2 + 4r + 2)N_{6\text{th}}^4 \\
&+ \gamma(48r^6 + 144r^5 + 312r^4 + 384r^3 \\
&+ 312r^2 + 144r + 48)N_{6\text{th}}^6
\end{aligned} \quad (14)$$

with respect to  $N_{6\text{th}}$ , we obtain  $N_{6\text{th}}$  and  $f_{2+4} + f_6$ . We plot  $N_{6\text{th}}$  and  $f_{2+4} + f_6$  as functions of  $r$  in Fig. 1. From this figure, we find that the case with  $r = -1/2$  is realized, which is the UN phase. At  $r = -1/2$ , we find  $N_{6\text{th}}$ :

$$N_{6\text{th}} = \sqrt{\frac{6\beta - \sqrt{(6\beta)^2 - 2784\alpha\gamma}}{1392|\gamma|}}. \quad (15)$$

In the UN phase, the unbroken symmetry is  $D_\infty \simeq O(2) = SO(2) \rtimes \mathbb{Z}_2$ , where  $\rtimes$  denotes a semi-direct product.

(3) Let us consider the case that we take into account the magnetic fields but without the sixth order term:  $f_{2+4} + f_H$ . Here, we consider the two cases for the magnetic fields; those along the  $z$  (poloidal) direction ( $\mathbf{H} \parallel \mathbf{z}$ ) and the angular (toroidal) direction ( $\mathbf{H} \parallel \boldsymbol{\theta}$ ). The second case may not be physical for the ground state but we use it for the boundary in the presence of a vortex in the next section. We can derive the ground state  $A_{\text{mag}}$

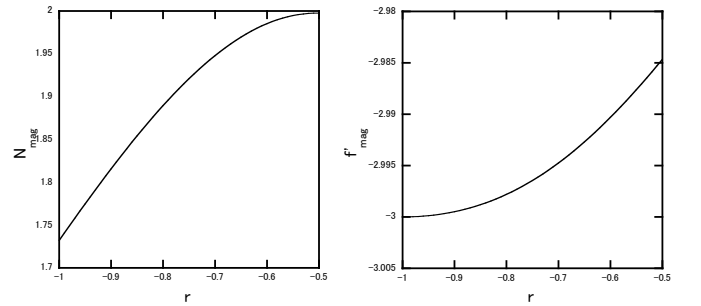


FIG. 2. The normalization and free energy  $f_{2+4} + f_H$ . Left panel: the normalization  $N_{\text{mag}}$  as a function of  $r$ . Right panel:  $f'_{\text{mag}}$  defined by  $f_{2+4} + f_H \equiv \frac{|\alpha|^2}{6\beta} f'_{\text{mag}}$  as a function of  $r$ . The  $D_4$  BN state with  $r = -1$  is the ground state.

with the same method as the case (2). Let us consider the magnetic field along the  $z$  axis. With the Ansatz,

$$A_{\text{mag}}^{(x,y,z)} = \sqrt{\frac{|\alpha|}{6\beta}} N_{\text{mag}} \begin{pmatrix} 1 & 0 & 0 \\ 0 & r & 0 \\ 0 & 0 & -(1+r) \end{pmatrix}, \quad (16)$$

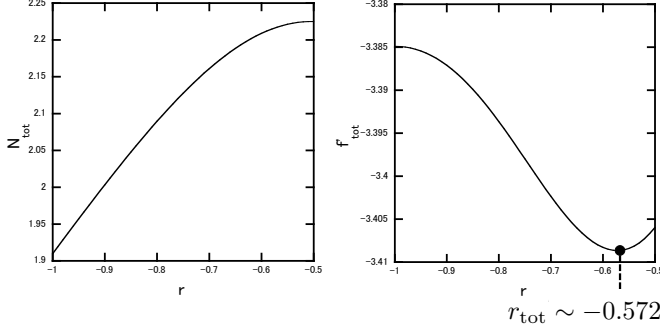


FIG. 3. The normalization and free energy  $f_{2+4} + f_6 + f_H$ . Left panel: the normalization  $N_{\text{tot}}$  as a function of  $r$ . Right panel:  $f'_{\text{tot}}$  defined by  $f_{2+4} + f_6 + f_H \equiv \frac{|\alpha|^2}{6\beta} f'_{\text{tot}}$  as a function of  $r$  (for  $H = 10^{15}$  Gauss). The intermediate state, the  $D_2$  BN state (with  $r \sim -0.572$  for  $H = 10^{15}$  Gauss), is the ground state.

we can minimize the free energy density

$$f_{2+4} + f_H = (2\alpha(1+r+r^2) + g_H H_z^2(1+r)^2) N_{\text{mag}}^2 + \beta(2r^4 + 4r^3 + 6r^2 + 4r + 2) N_{\text{mag}}^4 \quad (17)$$

with respect to  $N_{\text{mag}}$ . Fig. 2 shows  $N_{\text{mag}}$  and  $f_{2+4} + f_H$  that minimizing the free energy as functions of  $r$ . From this figure, we find that the case with  $r = -1$  is realized, which is the  $D_4$  BN phase.

To summarize, the ground state  $A_{\text{mag}}$  becomes

$$\begin{cases} A_{\text{mag}}^{(x,y,z)} = \sqrt{\frac{|\alpha|}{2\beta}} \begin{pmatrix} 1 & 0 & 0 \\ 0 & -1 & 0 \\ 0 & 0 & 0 \end{pmatrix} & (\mathbf{H} \parallel \mathbf{z}) \\ A_{\text{mag}}^{(\rho,\theta,z)} = \sqrt{\frac{|\alpha|}{2\beta}} \begin{pmatrix} 1 & 0 & 0 \\ 0 & 0 & 0 \\ 0 & 0 & -1 \end{pmatrix} & (\mathbf{H} \parallel \boldsymbol{\theta}) \end{cases} \quad (18)$$

The energy contribution from the magnetic fields vanish in these cases. The symmetry of this state is  $D_4$  symmetry, and we call this phase as the  $D_4$  BN phase [36, 40] [41].

(4) Finally, we consider the total free energy including the sixth order term and magnetic term ( $f_{2+4} + f_6 + f_H$ ), where we consider the magnetic field along the  $z$  axis. The intermediate states with the symmetry  $D_2$ , that we call the  $D_2$  BN phase, are realized. The order parameter has the following form

$$A^{(x,y,z)} = N_{\text{tot}} \begin{pmatrix} 1 & 0 & 0 \\ 0 & r & 0 \\ 0 & 0 & -1-r \end{pmatrix}. \quad (19)$$

The free energy density  $f_4 + f_6 + f_H$  can be written in

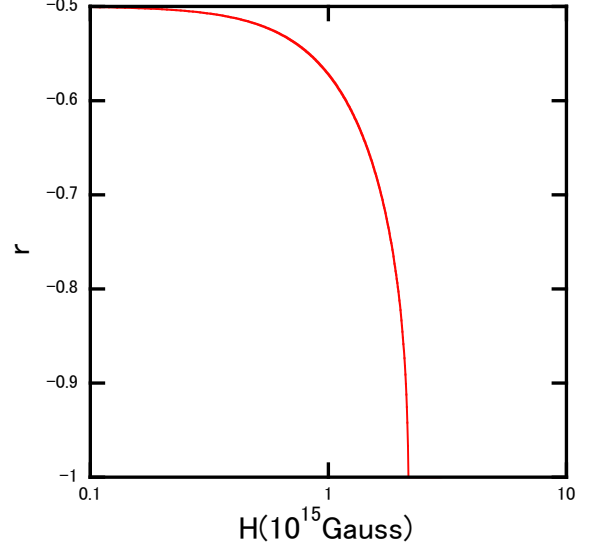


FIG. 4. The parameter  $r = r_{\text{tot}}(H)$  minimizing the free energy  $f_{2+4} + f_6 + f_H$  as a function of magnetic field  $H$ .

terms of the parameter  $r$  and  $N_{\text{tot}}$  as follows:

$$f_{2+4} + f_6 + f_H = (2\alpha(1+r+r^2) + g_H H_z^2(1+r)^2) N_{\text{tot}}^2 + \beta(2r^4 + 4r^3 + 6r^2 + 4r + 2) N_{\text{tot}}^4 + \gamma(48r^6 + 144r^5 + 312r^4 + 384r^3 + 312r^2 + 144r + 48) N_{\text{tot}}^6. \quad (20)$$

By minimizing this free energy density with respect to  $r$  and  $N_{\text{tot}}$ , we can obtain the ground state. In Fig. 3, we plot  $N_{\text{tot}}$  and the free energy density as a function of  $r$  with  $H = 10^{15}$  Gauss. In this case, the minimum free energy density can be achieved at

$$r \sim -0.572 \equiv r_{\text{tot}} \text{ for } H = 10^{15} \text{ Gauss}. \quad (21)$$

In Fig. 4, we plot  $r$  that minimizing the energy as a function of the strength of the magnetic field  $H$ . The ground state is in the UN phase for the weak magnetic field, while the  $D_4$  BN phase is realized for the strong magnetic field. The parameter  $r$  changes drastically around the magnetic field of  $10^{15}$  Gauss.

### III. VORTEX STRUCTURES IN $^3P_2$ SUPERFLUIDS

#### III.1. Vortex lattice

When superfluids are rotating, superfluid vortices are created along the rotation axis. In this section, we discuss vortices in the  $^3P_2$  superfluids. The existence of vortices in the  $^3P_2$  superfluids is topologically ensured by the first homotopy group summarized in Table II. The number  $N_v$  of vortices with the unit circulation created inside

rotating neutron stars can be estimated to be

$$N_v \sim 1.9 \times 10^{19} \left( \frac{1\text{ms}}{P} \right) \left( \frac{M^*}{900\text{MeV}} \right) \left( \frac{R}{10\text{km}} \right)^2 \quad (22)$$

where  $P$  is the period of the neutron star,  $M^*$  is the effective neutron mass, and  $R$  is the radius of the  ${}^3P_2$  superfluid. Then, we can estimate the distance between vortices  $d$  from

$$\pi d^2 \times N_v = \pi R^2, \quad (23)$$

that implies the intervortex distance  $d$  to be

$$d \sim 1.7 \times 10^{-6}\text{m} \quad (24)$$

for the typical values for  $P$ ,  $M^*$  and  $R$  in Eq. (22).

On the other hand, the coherence length  $\xi$  of  ${}^3P_2$  superfluid is about 10 – 100 fm. Therefore the distance between vortices is much larger than the coherence length, and therefore we consider a single vortex below.

### III.2. Vortex Ansatz and asymptotic energy of a vortex

Let us derive the equation of motion from the free energy  $F$  introduced in the last section. Here, we consider the following Ansatz for the order parameter of a vortex state:

$$A^{(x,y,z)} = \sqrt{\frac{|\alpha|}{6\beta}} R(n\theta) A^{(\rho,n\theta,z)} R^T(n\theta) e^{il\theta},$$

$$A^{(\rho,n\theta,z)} = \begin{pmatrix} f_1 & i g e^{im\theta+i\delta} & 0 \\ i g e^{im\theta+i\delta} & f_2 & 0 \\ 0 & 0 & -f_1 - f_2 \end{pmatrix} \quad (25)$$

in the cylindrical coordinates  $(\rho, \theta, z)$ , where  $l, m, n$  are integers,  $l, m, n \in \mathbb{Z}$ , explained below,  $\delta$  is a constant,  $A^{(x,y,z)}$  is the order parameters in the Cartesian basis and  $A^{(\rho,n\theta,z)}$  is the order parameters in the cylindrical basis ( $n = 1$ ) or its higher generalizations, which are related by a rotation matrix  $R$ , given by

$$R(n\theta) = \begin{pmatrix} \cos n\theta & -\sin n\theta & 0 \\ \sin n\theta & \cos n\theta & 0 \\ 0 & 0 & 1 \end{pmatrix}. \quad (26)$$

In Eq. (25),  $f_1, f_2, g$  are profile functions depending only on the radial coordinate  $\rho$ , and the boundary conditions for them are

$$f_1, f_2 \rightarrow \text{constant}, \quad g \rightarrow 0 \quad \text{as } \rho \rightarrow \infty,$$

$$f_1, f_2 \rightarrow 0, \quad \begin{cases} g \rightarrow 0 \text{ for } n \neq -1 \\ g' \rightarrow 0 \text{ for } n = -1 \end{cases} \quad \text{as } \rho \rightarrow 0, \quad (27)$$

where the case of  $n = -1$  is exceptional since the the total winding of  $g$  vanishes. As denoted, the configuration is labeled by the three integers  $l, m, n \in \mathbb{Z}$ , where  $l$  is the winding number of the vortex,  $n$  represents a rotation of  $SO(3)$  that does not have a topological nature, and  $m$

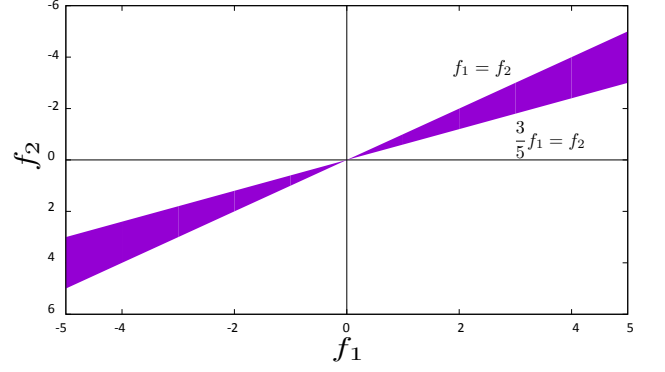


FIG. 5. The conditions for determining whether the Cartesian basis or cylindrical basis is realized. The cylindrical basis ( $n = 1$ ) is realized in the shaded area while the Cartesian basis ( $n = 0$ ) is realized in the rest.

is a semi-topological winding number (relative to that of  $f_{1,2}$ ) defined locally for the component  $g$  [42].

Let us consider the tension, the energy per unit length, of the vortex. A bulk part of free energy density,  $f_{2+4} + f_6 + f_H$ , does not depend on the integers  $l, m, n$ , while the gradient term depends on them; The leading contribution to the gradient energy at large  $\rho$  depends on  $n$  and  $l$  as follows:

$$F = \int d^2\rho \frac{1}{\rho^2} [2K_1(l^2(f_1^2 + f_1 f_2 + f_2^2) + n^2(f_1 - f_2)^2) + 2K_2(f_1^2 \sin^2(n-1)\theta + f_2^2 \cos^2(n-1)\theta) + n^2(f_1 - f_2)^2]$$

$$\sim 2\pi \log L$$

$$\times [2K_1(l^2(f_1^2 + f_1 f_2 + f_2^2) + n^2(f_1 - f_2)^2) + \begin{cases} 2K_2(l^2 f_2^2 + n^2(f_1 - f_2)^2) & (n = 1) \\ K_2(l^2(f_1^2 + f_2^2) + 2n^2(f_1 - f_2)^2) & (n \neq 1) \end{cases}] \quad (28)$$

where  $\sim$  denotes the asymptotic form and  $L$  is the system size transverse to the vortex, and  $f_1$  and  $f_2$  in the last line are the boundary values evaluated at  $\rho \rightarrow \infty$ .

From this equation, we first see that the configuration with  $l = 1$  has the lower energy than the configuration with higher winding numbers  $l > 1$ , as for conventional superfluids, thereby a vortex with the higher winding  $l$  is unstable to be split into  $l$  unit winding vortices. In the following, we concentrate on  $l = 1$ .

As for  $n$ , we find that either the case of  $n = 0$  (the  $xyz$ -basis) or of  $n = 1$  (the cylindrical basis) gives the lowest free energy. The condition on  $f_1$  and  $f_2$  that determines which configuration with  $n = 0$  or  $n = 1$  has lower energy is plot in Fig. 5, where the cylindrical basis ( $n = 1$ ) gives lower energy in the shaded region defined by

$$\frac{3}{5}f_1 < f_2 < f_1, \quad (29)$$

while the  $xyz$  basis ( $n = 0$ ) gives lower energy in the rest.

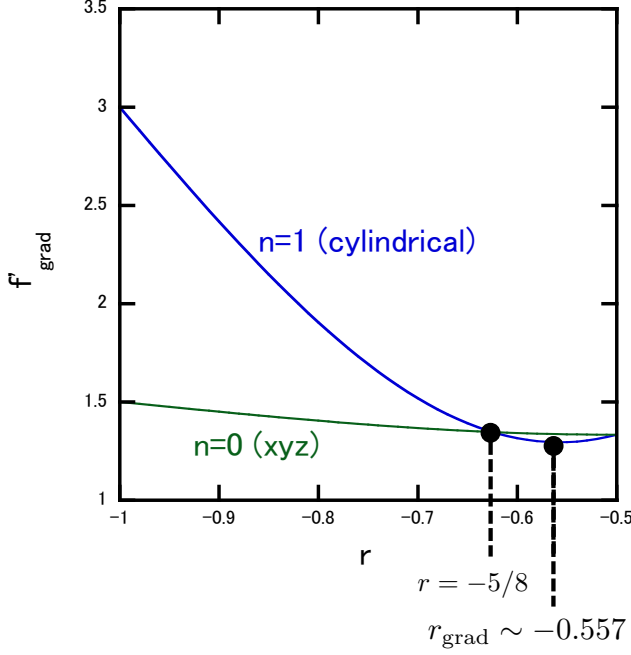


FIG. 6. The leading contribution to the free energy  $F \sim 2\pi K_1 \log L \times f'_{\text{grad}}$  in Eq. (28) as functions of the parameter  $r$  at the infinity for the  $n = 0$  (purple curve) and  $n = 1$  (green curve) cases, which cross at  $r = -5/8$ . The minimum point is  $r_{\text{grad}} = 6 - \sqrt{43}$  for  $n = 1$  in Eq. (41).

This condition can also be translated in terms of the parameter  $r$ . If  $f_2^2 \leq f_1^2 \leq (f_1 - f_2)^2$  is not satisfied, the configuration with  $n = 0$  always give the least energy state. Therefore, if  $n = 1$  is realized, the order parameter becomes the following form

$$A^{(x,y,z)} \propto \sqrt{\frac{1}{r^2 + r + 1}} R(n\theta) \begin{pmatrix} r & 0 & 0 \\ 0 & -1 - r & 0 \\ 0 & 0 & 1 \end{pmatrix} R^T(n\theta) e^{i\theta} \quad (30)$$

In Fig. 6, we plot the leading contribution to the free energy proportional to  $\log L$  in Eq. (28) as a function of  $r$  for the cases of  $n = 0$  (purple curve) and  $n = 1$  (green curve). From this figure, we can see that the configuration of  $n = 1$  has the lower energy in the region  $-5/8 \leq r \leq -1/2$ . At the cross point  $r = -5/8$ , there is a first order phase transition. In the following, we consider only the cases of  $n = 0$  and  $n = 1$ .

### III.3. Tension of a vortex

We calculate the free energy per the unit vortex length analytically for each basis:

$$F = \int d^2\rho \frac{|\alpha|}{6\beta} (K_1 t_1 + K_2 t_2 + \alpha t_3 + \frac{|\alpha|}{6\beta} \beta t_4 + \frac{\alpha^2}{36\beta^2} \gamma t_5) \quad (31)$$

where the terms  $t_1$  and  $t_2$  come from the gradient terms and the terms  $t_3$ ,  $t_4$  and  $t_5$  come from the second, fourth and sixth order terms, respectively, in the GL free energy density in Eq. (6). Here  $t_{1,2}$  can be written in the cylindrical basis as

$$t_1^{(\rho,\theta,z)} = 2(f_1'^2 + f_2'^2 + f_1'f_2' + g'^2) + \frac{1}{\rho^2} (4f_1^2 + 4f_2^2 - 2f_1f_2 + (8 + 2(m+1)^2)g^2 - 4(f_1 - f_2)g(m+2)\cos(m\theta + \delta)), \quad (32)$$

$$t_2^{(\rho,\theta,z)} = 2(f_1'^2 + g'^2) + \frac{2}{\rho^2} (f_2^2 + 4g^2 + (m+1)^2g^2 + (f_1 - f_2)^2 - 2g(m+1)(f_1 - f_2)\cos(m\theta + \delta) + 4f_2g\cos(m\theta + \delta)) + \frac{1}{\rho} (-2(f_1' + f_2')g(m+1)\cos(m\theta + \delta) + 2(f_1 + f_2)g'\cos(m\theta + \delta) + 2(f_1' + f_2')(f_1 - f_2)), \quad (33)$$

and in the  $xyz$  basis as

$$t_1^{(x,y,z)} = 2(f_1'^2 + f_2'^2 + f_1'f_2' + g'^2) + \frac{2}{\rho^2} (f_1^2 + f_2^2 + f_1f_2 + (m+1)^2g^2), \quad (34)$$

$$t_2^{(x,y,z)} = 2(\cos^2\theta f_1'^2 + \sin^2\theta f_2'^2 + g'^2) + \frac{2}{\rho^2} (\sin^2\theta f_1^2 + \cos^2\theta f_2^2 + (m+1)^2g^2) - 2\sin 2\theta \sin(m\theta + \delta)(f_1' + f_2')g' - \frac{2}{\rho} \cos 2\theta \cos(m\theta + \delta)(m+1)(f_1' + f_2')g + \frac{2}{\rho} \cos 2\theta \cos(m\theta + \delta)(f_1 + f_2)g' + \frac{2}{\rho^2} \sin 2\theta \sin(m\theta + \delta)(m+1)(f_1 + f_2)g. \quad (35)$$

The rest terms of the free energy density  $t_{3,4,5}$  can be written in the both basis as

$$t_3 = 2(f_1^2 + f_2^2 + f_1f_2 + g^2), \quad (36)$$

$$t_4 = 2f_1^4 + 4f_1^3f_2 + 6f_1^2f_2^2 + 4f_1 + f_2^3 + 2f_2^4 + ((6 + 2\cos 2(m\theta + \delta))f_1^2 + 4f_1f_2 + (6 + 2\cos 2(m\theta + \delta))f_2^2)g^2 + 2g^4, \quad (37)$$

	Case (1)	Case (2)	Case (3a)	Case (3b)	Case (4)
Phase	$D_2$ BN	UN	$D_4$ BN	$D_4$ BN	$D_2$ BN (or UN, $D_4$ BN)
$\begin{pmatrix} f_1 \\ f_2 \\ -f_1 - f_2 \end{pmatrix}$ at $\rho \rightarrow \infty$	$\begin{pmatrix} r_{\text{grad}} & & \\ & -1 - r_{\text{grad}} & \\ & & 1 \end{pmatrix}$	$\begin{pmatrix} 1 & & \\ & 1 & \\ & & -2 \end{pmatrix}$	$\begin{pmatrix} 1 & & \\ & 0 & \\ & & -1 \end{pmatrix}$	$\begin{pmatrix} 1 & & \\ & -1 & \\ & & 0 \end{pmatrix}$	$\begin{pmatrix} 1 & & \\ & r_{\text{tot}} & \\ & & -1 - r_{\text{tot}} \end{pmatrix}$
Basis	$n = 1$	$n = 0$ (or 1)	$n = 1$	$n = 0$	$n = 0$
Situation ( $f_{\text{grad}} + f_{2+4}$ plus)	non	$f_6$	$f_{H(\parallel\theta)}$	$f_{H(\parallel z)}$	$f_6 + f_{H(\parallel z)}$

TABLE III. The boundary conditions and physical situation for each case.  $r_{\text{grad}} \equiv 6 - \sqrt{43} \sim -0.557$  given in Eq. (41), and  $r_{\text{tot}}$  depends on the magnetic field ( $r_{\text{tot}} \sim -0.572$  in Eq. (21) for  $H = 10^{15}$  Gauss).

$$\begin{aligned}
t_5 = & 48f_1^6 + 144f_1^5f_2 + 312f_1^4f_2^2 + 384f_1^3f_2^3 \\
& + 312f_1^2f_2^4 + 144f_1f_2^5 + 48f_2^6 + 48g^6 \\
& + ((288 + 144\cos 2(m\theta + \delta))f_1^4 \\
& + (360 + 120\cos 2(m\theta + \delta))f_1^3f_2 \\
& + (576 + 240\cos 2(m\theta + \delta))f_1^2f_2^2 \\
& + (360 + 120\cos 2(m\theta + \delta))f_1f_2^3 \\
& + (288 + 144\cos 2(m\theta + \delta))f_2^4)g^2 \\
& + ((288 + 120\cos 2(m\theta + \delta))f_1^2 \\
& + (144 - 48\cos 2(m\theta + \delta))f_1f_2 \\
& + (288 + 120\cos 2(m\theta + \delta))f_2^2)g^4. \tag{38}
\end{aligned}$$

The effect of  $\delta$  on the free energy density is not clear. In this paper, we restrict the case with  $\delta = 0$ , which is consistent with the equation of motion, since the imaginary part of non-diagonal elements is directly connected with real part of diagonal elements through the equation of motion. By substituting the order parameter into Eq. (6) and differentiating it with respect to  $f_1$ ,  $f_2$  and  $g$ , we obtain the sets of the equation of motions for each basis, as summarized in Appendix B.

### III.4. Vortex solutions

In this paper, we construct the vortex configurations in the following five cases:

- Case (1):  $F = \int d^2\rho f_4$
- Case (2):  $F = \int d^2\rho (f_4 + f_6)$
- Case (3a):  $F = \int d^2\rho (f_4 + f_H)$  and  $\mathbf{H} \parallel \boldsymbol{\theta}$ .
- Case (3b):  $F = \int d^2\rho (f_4 + f_H)$  and  $\mathbf{H} \parallel \mathbf{z}$ .
- Case (4):  $F = \int d^2\rho (f_4 + f_6 + f_H)$  and  $\mathbf{H} \parallel \mathbf{z}$ .

We summarize the forms of the order parameters in these cases in Table III. In numerical simulations, we change the variable  $\rho$  ( $0 \leq \rho < \infty$ ) by  $\tanh\rho$  ( $0 \leq \tanh\rho < 1$ ). We divide the domain of  $\tanh\rho$  into 100 parts and solve the equations of motion given in Appendix B simultaneously by using the Newton's method.

#### Case (1)

This is only the case studied before [14, 18, 19]. This case may be thought to be unphysical because of the

presence of the sixth order term, but it is relevant when the gap is small enough ( $f_6$  is much smaller than  $f_4$ ) and the magnetic field is small compared with  $f_4$ . In this case, the ground state takes the form in Eq. (11) due to the fourth order term. We can see from Eq. (28) that the leading part of free energy proportional to  $\log L$  becomes lower when  $f_2^2 \leq f_1^2$ , so that we take the following order parameter form

$$\begin{aligned}
& A^{(x,y,z)} \\
& \propto \sqrt{\frac{1}{r^2 + r + 1}} R(n\theta) \begin{pmatrix} r & 0 & 0 \\ 0 & -1 - r & 0 \\ 0 & 0 & 1 \end{pmatrix} R^T(n\theta) e^{i\theta} \tag{39}
\end{aligned}$$

with  $-1 \leq r \leq -1/2$ . Let us assume that the ground state is in the cylindrical basis ( $n = 1$ ) from Fig. 6. By putting the order parameter into Eqs. (33) and (33), we obtain

$$F \propto \frac{9r^2 + 10r + 3}{r^2 + r + 1} \log L. \tag{40}$$

Then, by differentiating this free energy with respect to  $r$ , we get [14, 18, 19]

$$r = 6 - \sqrt{43} \sim -0.557 \equiv r_{\text{grad}} \tag{41}$$

that satisfies  $-5/8 < r_{\text{grad}} < -1/2$ , and so the lowest energy state is in the cylindrical basis ( $n = 1$ ) consistently. It is interesting to emphasize that the particular  $r$  is selected as the vortex boundary state although the ground states are continuously degenerate with  $r$ .

Let us make a comment on the case of spin-2 BECs for which the gradient term consists of only the first term proportional to  $K_1$  with  $K_2 = 0$ . In this case, the boundary becomes the UN phase with  $r = -1/2$  (up to the fourth order). This phenomenon of selection of the vortex boundary state is not known in the context of BEC. The quasi-NG mode is gapped through the gradient term in the presence of a vortex.

In Fig. 7, we plot the profiles functions  $f_1$ ,  $f_2$  and  $g$  as functions of the distance  $\rho$  from the vortex center. The red curves correspond to the case of  $m = 0$  with  $g \neq 0$ , which is the case considered in Ref. [19] without explicit solutions. The new solution here is the case with  $g = 0$  represented by the black curves. We see that all the terms in the equation of motion for  $g$  [Eq. (B3) in Appendix B] contain  $g$  if  $m \neq 0$ . Consequently, in this



case,  $g = 0$  is a trivial solution in the entire region of  $\rho$  since  $g$  is fixed to be zero at the both boundaries. This implies that all  $m \neq 0$  give the same solution of  $g = 0$ . In order to determine which state between  $g \neq 0$  (with  $m = 0$ ) and  $g = 0$  has less energy, we should compare the free energies for these two cases, but we leave it as a future problem.

#### Case (2)

As we discussed before, if we add the sixth order term, the ground state is in the UN phase. Since  $f_1 = f_2$  is the boundary between the cases with  $n = 0$  and  $n = 1$  (see Fig. 4), we cannot determine the basis easily. However, by considering the rotational energy from the basis, we take  $n = 0$  in this paper. Fig. 8 shows  $f_1$ ,  $f_2$  and  $g$  as functions of  $\rho$ . In this situation, we find from Eq. (B6) in Appendix B that  $g = 0$  is a trivial solution in the entire region of  $\rho$  except for the cases of  $m = \pm 2$ . This implies that all  $m(\neq \pm 2)$  give the same solution. In the  $n = 0$  basis, the equation of motions for  $f_1$  and  $f_2$  have the same form. Since  $f_1 = f_2$  is satisfied at the boundary as we have already mentioned,  $f_1 = f_2$  holds at all  $\rho$  for any  $m$ . The blue and green curves correspond to the cases of  $g \neq 0$  with  $m = 2$  and  $m = -2$ , respectively, while the black curves represent for the case of  $g = 0$ . In the figures for  $f_1$  and  $f_2$ , we cannot see the differences among all the cases but they have tiny differences numerically.

#### Cases (3a) and (3b)

Let us consider the cases that external magnetic fields are present either along the  $\theta$  direction encircling the vortex [the case (3a)] or along the vortex direction [the case (3b)].

When the magnetic field along the  $\theta$  direction is present, the  $D_4$  BN phase in the cylindrical ( $n = 1$ ) basis is realized as the boundary state. We plot  $f_1$ ,  $f_2$  and  $g$  as functions of  $\rho$  in Fig. 9. In the  $n = 1$  basis, from the same reason as the case (1), only the case with  $m = 0$  has a non-zero value for  $g$ . The red and black curves correspond to the cases of  $g \neq 0$  (with  $m = 0$ ) and  $g = 0$ , respectively.

When the magnetic field along the  $z$  axis is present, we obtain the  $D_4$  BN phase as the boundary state of the vortex as shown in Eq. (18). Since  $f_1 = -f_2$  holds at the boundary  $\rho \rightarrow \infty$ , we find from Fig. 4 that the boundary state is in the Cartesian ( $n = 0$ ) basis. Fig. 10 shows the profile functions  $f_1$ ,  $f_2$  and  $g$  as functions of  $\rho$  in the case (3b). Since the relation  $f_1 = -f_2$  is satisfied at the two boundaries and the equation of motions for  $f_1$  and  $f_2$  take the same form, the relation  $f_1 = -f_2$  holds in the entire region of  $\rho$ . Consequently, the terms proportional to  $\frac{\partial^2 f_{1(2)}}{\partial \rho^2}$  and  $\frac{\partial f_{1(2)}}{\rho \partial \rho}$  vanish. As a result,  $g$  has a trivial solution  $g = 0$  for all  $m$ , implying that all  $m$  give the identical solution.

In the cases (3a) and (3b), the ground state does not depend on the magnitude of the magnetic field, while the profile of vortices of course depends on the magnitude of the magnetic field. We set the magnetic field to be  $10^{15}$  Gauss, which corresponds to magnetars. To realize the

situations in the cases (3a) and (3b), we need a strong magnetic field larger than about  $3 \times 10^{15}$  Gauss as can be seen from Fig. 4. Therefore, the value  $10^{15}$  Gauss is not appropriate, but the qualitative behaviors of vortex profiles are not changed even when we change the magnitude of the magnetic field to  $10^{16-17}$  Gauss.

#### Case (4)

Finally, let us consider the most realistic case for neutron stars, that is, the case with the sixth order term in the presence of the magnetic field of  $10^{15}$  Gauss along the  $z$  axis. This case reduces to the case (2) in the absence of the magnetic field and to the case (3b) in the presence of strong magnetic field for which the sixth order term is negligible.

In this case, the smallest eigenvalue  $-1 - r$  comes to the  $z$  component. By using Fig. 4, we can see that the  $xyz$  basis ( $n = 0$ ) is realized. By minimizing Eq. (20), we have  $r = r_{\text{tot}} \sim -0.572$  in Eq. (21) as the boundary condition at large distance.

In Fig. 11, we plot  $f_1$ ,  $f_2$  and  $g$  as functions of  $\rho$  with  $m = -2, \dots, 2$  in the case (4). For the same reason as the case (2), only the cases with  $m = \pm 2$  have a non-zero value for  $g$ . The blue, green and black curves correspond to the cases of  $g \neq 0$  with  $m = 2$ ,  $g \neq 0$  with  $m = -2$ , and  $g = 0$ , respectively. In figures for  $f_1$  and  $f_2$ , the cases of  $g \neq 0$  with  $m = \pm 2$  and of  $g = 0$  take the different values numerically although they are almost overlapped.

### IV. SPONTANEOUS MAGNETIZATION OF THE $^3P_2$ VORTEX CORE

In this section, we calculate the spontaneous magnetization of  $^3P_2$  vortex cores due to the neutron anomalous magnetic moment for the vortex profiles obtained in the last section. The spontaneous magnetization was already reported in the case (1) [19]. This is a characteristic feature of  $^3P_2$  vortices that is absent for conventional  $^1S_0$  vortices. The vortex magnetization  $\mathbf{M}(\rho)$  can be calculated as

$$\begin{aligned} \mathbf{M} &= \frac{\gamma_n \hbar}{2} \hat{\sigma}, \\ \hat{\sigma} &= T \sum_n \int \frac{d^3 k}{(2\pi)^3} \text{Tr}(\sigma G(k, \omega_n)) \\ &= \int \frac{d\Omega}{4\pi} \text{Tr}(\sigma \Delta \Delta^\dagger) T \sum_n \int d\xi N(0) \frac{i\omega_n + \xi}{(\omega_n^2 + \xi^2)^2} \\ &= \frac{4}{9} N'(0) k_F^2 \frac{|\alpha|}{6\beta} g(\rho) (f_1(\rho) - f_2(\rho)) \cos m \theta \hat{z} \end{aligned} \quad (42)$$

where  $G(k, \omega_n)$  is a thermal Green function and  $\omega_n = (2n + 1)\pi T$  is the Matsubara frequency and  $N'(0) = \frac{M^2}{2\pi^2 k_F}$  is the density of states differentiated by the energy  $E = k^2/2M$ ,  $N' = \frac{M^2}{2\pi^2 k}$ , evaluated at the Fermi surface  $k = k_F$ .

By using the results of the last section, we obtain the magnetization  $\mathbf{M}$  as a function of  $\rho$ . We plot  $M_z$  (for

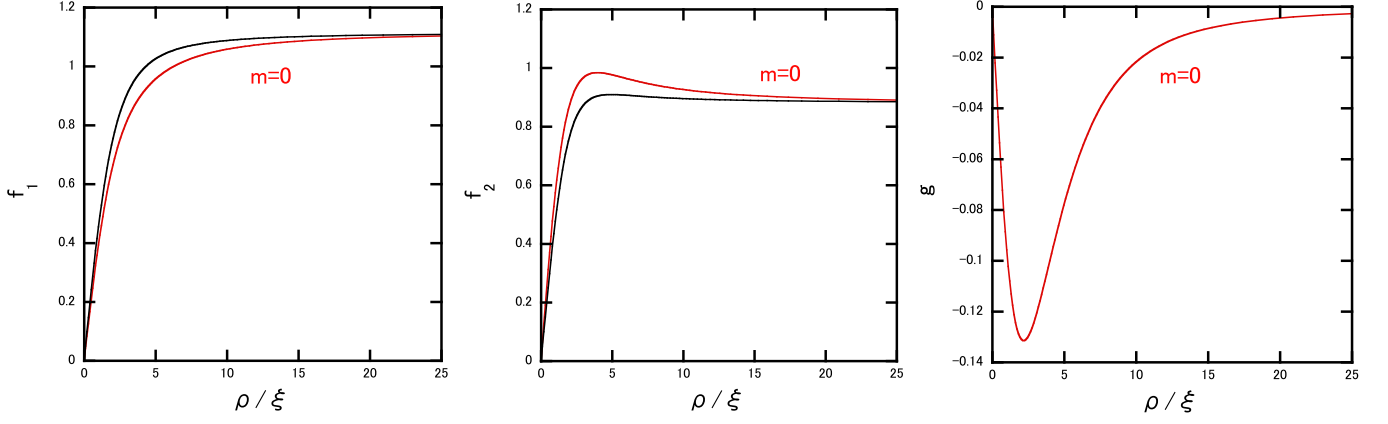


FIG. 7. The profile functions  $f_1$ ,  $f_2$  and  $g$  as functions of the distance  $\rho/\xi$  from the vortex center in the case (1). The red and black curves correspond to the cases of  $g \neq 0$  with  $m = 0$  and  $g = 0$ , respectively.

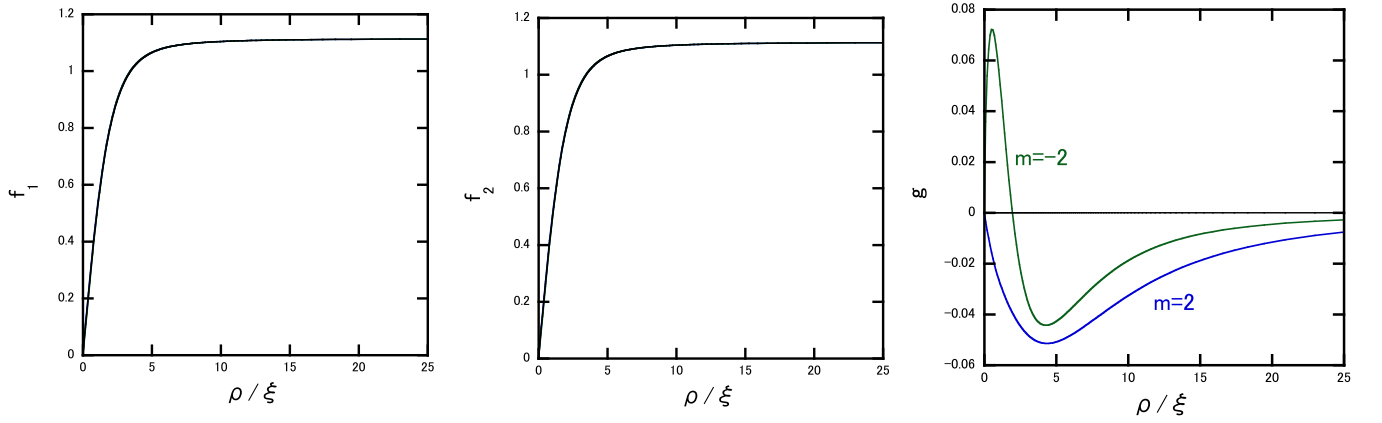


FIG. 8. The profile functions  $f_1$ ,  $f_2$  and  $g$  as functions of the distance  $\rho/\xi$  from the vortex center in the case (2). The profile functions  $f_1$  and  $f_2$  are identical:  $f_1 = f_2$  in this case. The blue, green black curves correspond to the cases of  $g \neq 0$  with  $m = 2$ ,  $g \neq 0$  with  $m = -2$  and  $g = 0$ , respectively. All the cases take different values numerically although the profiles of  $f_1$  and  $f_2$  are almost overlapped.

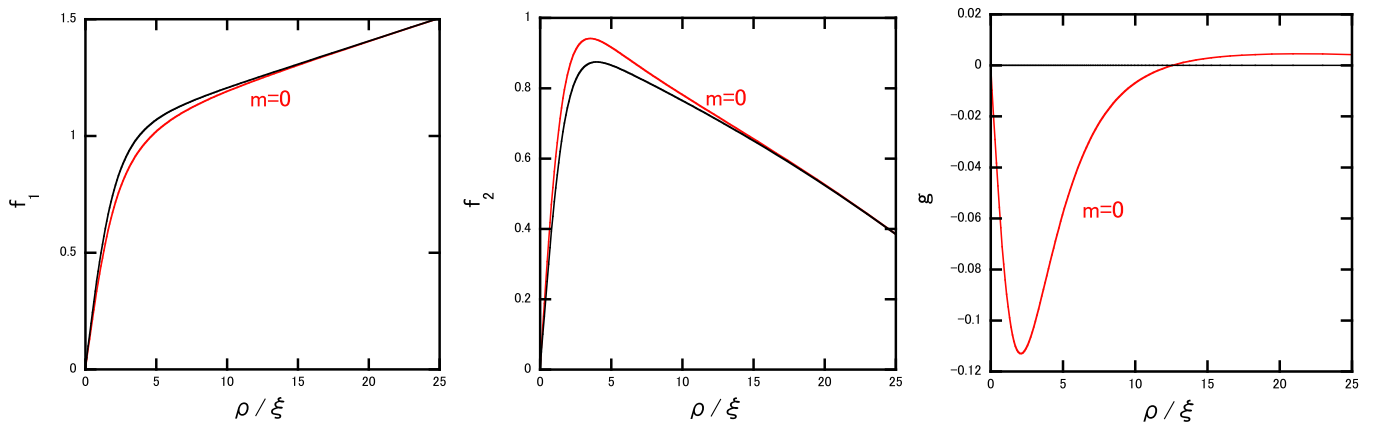


FIG. 9. The profile functions  $f_1$ ,  $f_2$  and  $g$  as functions of the distance  $\rho/\xi$  from the vortex center in the case (3a). The red and black curves correspond to the cases of  $g \neq 0$  with  $m = 0$  and  $g = 0$ , respectively.

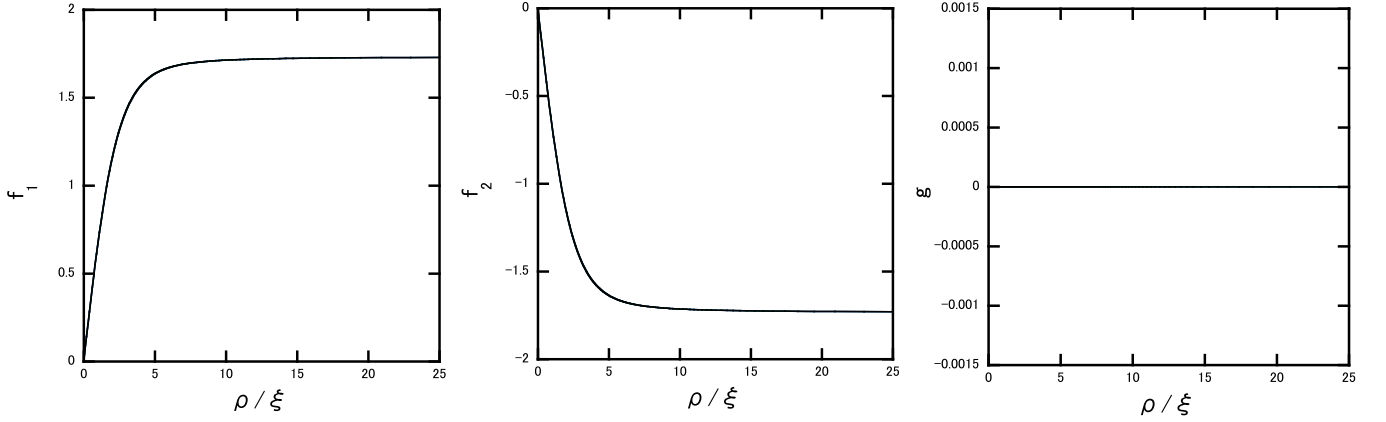


FIG. 10. The profile functions  $f_1$ ,  $f_2$  and  $g$  as functions of the distance  $\rho/\xi$  from the vortex center in the case (3b). All  $m$  result in the same solution.

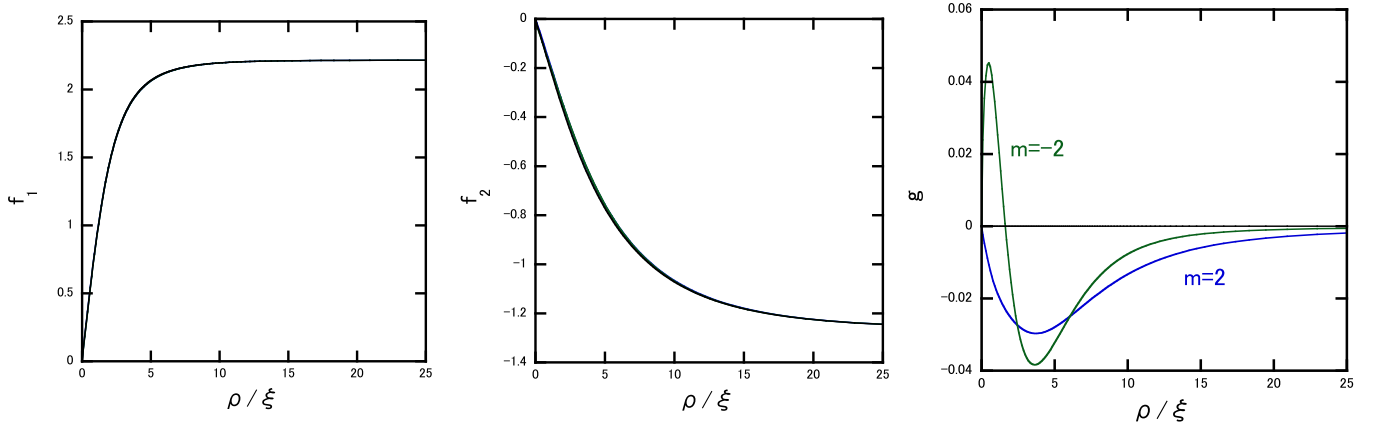


FIG. 11. The profile functions  $f_1$ ,  $f_2$  and  $g$  as functions of the distance  $\rho/\xi$  from the vortex center in the case (4). The blue, green and black curves correspond to the cases of  $g \neq 0$  with  $m = 2$ ,  $g \neq 0$  with  $m = -2$  and  $g = 0$ , respectively. In the figures of  $f_1$  and  $f_2$ , all the cases take the different values numerically.

$\theta = 0$ ) as functions of  $\rho$  for the cases (1)–(4) in Fig. 12. The red, blue and green curves correspond to the cases of  $g \neq 0$  with  $m = 0$ ,  $m = 2$  and  $m = -2$ , respectively, while the black curves correspond to the case of  $g = 0$ . The maximum value of  $M_z$  is about  $10^8$ - $10^9$  Gauss when it is nonzero. The mean magnetic field in a vortex lattice, which is obtained roughly by multiplying  $(\xi/d)^2 \sim 10^{-14}$ , is much smaller than the observed magnetic field about  $10^{12}$ - $10^{15}$  Gauss, and consequently this magnetic field is negligible.

Note that the magnetization  $M_z$  is proportional to  $(f_1(\rho) - f_2(\rho))g(\rho)\cos m\theta$ . Since it is proportional to the off-diagonal profile function  $g$  appearing around the vortex cores, it is nonzero only for the cases of  $m = 0$  in the  $xyz$ -basis and of  $m = \pm 2$  in the cylindrical basis. When  $f_1 \neq f_2$  in the region  $g \neq 0$ , the magnetization can occur. However, in the case (2), as we have already discussed,  $f_1 = f_2$  is satisfied for all  $\rho$ , and the magnetization  $M_z$  vanishes. Among all the cases with nonzero magnetization  $M_z$ , only the case with  $m = 0$  has a net

magnetization, since the  $\theta$  integration of  $\cos m\theta$  vanishes for  $m \neq 0$ . Although the case of  $m = \pm 2$  in the cylindrical basis has no net magnetization, the direction of the magnetization drastically changes upward and downward depending on  $\theta$ , thereby implying the existence of the large current crossing to the vortex.

## V. SUMMARY AND DISCUSSION

We have determined the ground states of the  $^3P_2$  superfluids in the presence of the external magnetic fields and have obtained the vortex solutions in various situations in the absence and presence of magnetic fields along the vortex axis or the angular direction. First, the boundary state at  $\rho \rightarrow \infty$  has been determined to lower the bulk free energy. Second, the basis diagonalizing the order parameter  $A_{\mu i}$  has been determined by the leading contribution to the gradient energy proportional to  $\log L$  and the coefficients  $K_1$  and  $K_2$ . The presence of the

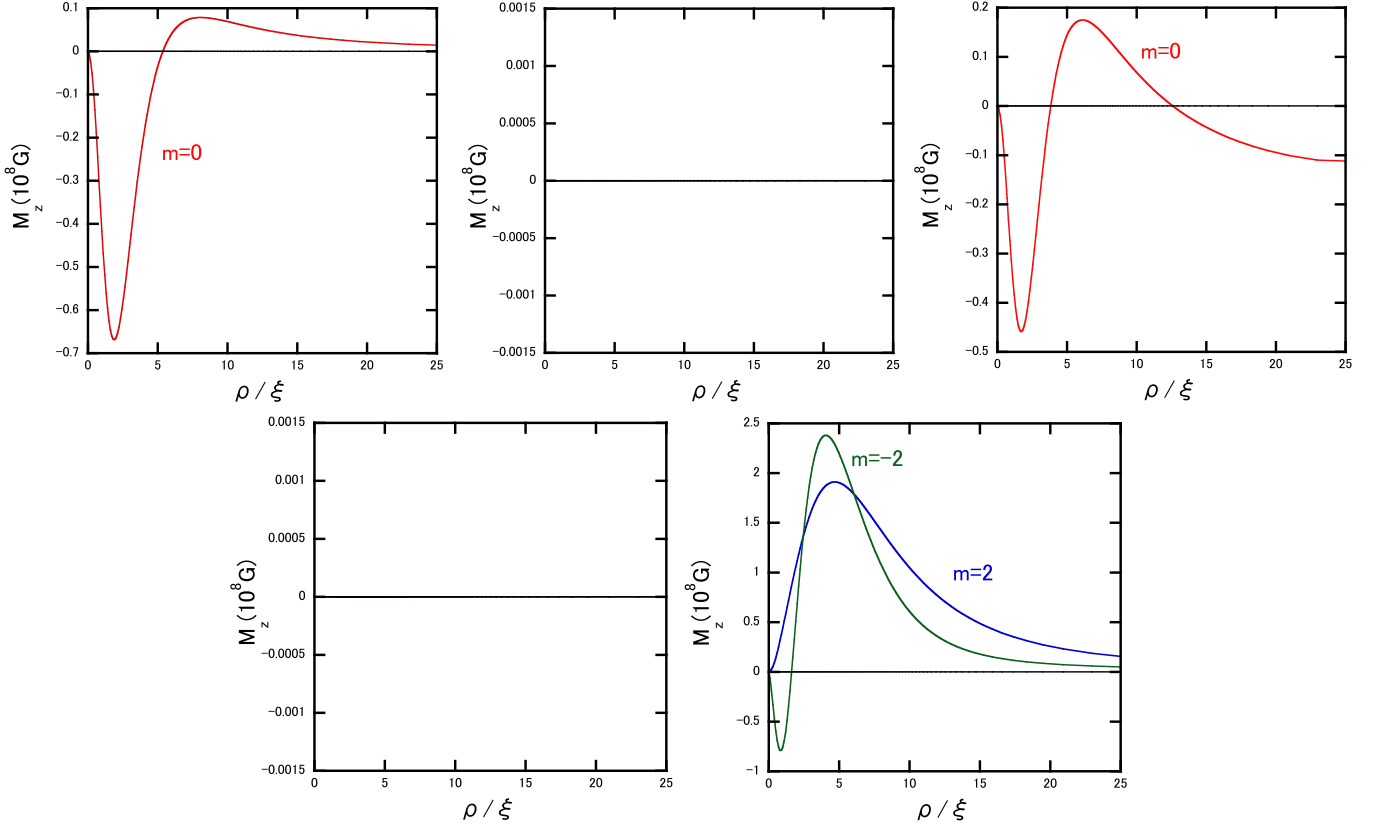


FIG. 12. The dependence of the magnetizations  $M_z$  on the distance  $\rho/\xi$  from the vortex core in the cases (1), (2), (3a), (3b) and (4). The red, blue and green curves correspond to the cases of  $m = 0$ ,  $m = 2$  and  $m = -2$  with  $g \neq 0$ , respectively, while the black lines correspond to the case with  $g = 0$  in the cases (1), (3a), (3b) and (4). The magnetization  $M_z$  vanishes in the case (2) because of  $f_1 = f_2$  even for  $g \neq 0$ .

gradient energy proportional to  $K_2$  is essential for the  ${}^3P_2$  superfluids unlike the spinor BEC for which such the terms are absent. In the absence of the magnetic field and the sixth order term, the ground state is continuously degenerate with the parameter  $r$ . Nevertheless the boundary value  $r$  for the vortex state is fixed and the cylindrical basis is realized due to the gradient energy. We have constructed the free energy density and equation of motion for the  $xyz$ -basis and cylindrical basis. By using the Ansatz of the vortex profiles with the non-diagonal component  $g$  which has the local winding number  $m$  relative to that of  $f_{1,2}$ , we have constructed the vortex profiles and have found that  $g$  is non-zero around the vortex core only for  $m = 0$  in the cylindrical basis and  $m = \pm 2$  in the  $xyz$ -basis. The former was known before without explicit profiles [14, 18, 19] for which we have given the explicit solution. As a result, the spontaneous magnetization around the vortex cores proportional to  $g \cos m\theta$  is present for these cases. The net magnetization survives for  $m = 0$  in the cylindrical basis, while in the case of  $m = \pm 2$  in the  $xyz$ -basis the net magnetization vanishes with local magnetization upward and downward depending on the angle coordinates. The typical value for the spontaneous magnetization is about  $10^8$  Gauss, which is much smaller than the neutron star observations.

Here we address some discussion. The unbroken symmetry is  $D_4$  for the  $D_4$  BN phase realized in the cases (3a) and (3b). Since the element of the  $D_4$  group consists of an element of simultaneous action of a  $U(1)$  phase rotation by  $\pi$  and an  $SO(3)$  rotation by  $\pi/2$ , the most fundamental vortex is a half-quantized vortex. In the BN phase, a single integer vortex discussed in this paper may be unstable against the decay into two half quantized vortices. The half quantized vortices belong to the non-Abelian first homotopy group  $D_4^*$  as in Table II. When two vortices characterized by elements that do not commute with each other collide, a bridge between them must be created [43], see Ref. [44] for such a collision dynamics in spinor BEC. We should consider the effects of the half quantized vortices in the  ${}^3P_2$  neutron superfluids.

We have discussed only vortices characterized by the first homotopy group. On the other hand, in Table II, we summarized higher homotopy groups that allow higher codimensional topological objects like monopoles, Skyrmions and so on.

It was argued in [45] that in helium 3 superfluid, the  $SO(3)$  symmetry unbroken in the ground state is further spontaneously broken around the core of an integer vortex due to the gradient term proportional to  $K_2$ , giving rise to (quasi-) gapless mode localized along the vortex.

The same discussion may be made for the integer vortex in the  ${}^3P_2$  superfluids studied in this paper.

In order to study the fermionic degree of freedom, the Bogoliubov-de-Gennes equation should be used beyond the GL free energy. It will turn out to be useful to show topological properties of the  ${}^3P_2$  superfluidity such as topological superfluidity and fermion zero modes trapped inside the vortex core.

The interface between  ${}^1S_0$  and  ${}^3P_2$  superfluids should be important to consider; in particular how vortices are connected in the both region. On the other hand, at much higher density, quark matter may appear such as color superconductors [46], where there exist  $1/3$  quantized superfluid vortices that carry color magnetic fluxes [47–51], the boojum structure on which vortices join will appear at the interface [52]. Dynamics of vortices at such the interfaces ( ${}^1S_0$ - ${}^3P_2$  and  ${}^3P_2$ -quark matter) may be important for dynamics of neutron stars.

### ACKNOWLEDGMENTS

We thank Tatsuyuki Takatsuka, Tetsuo Hatsuda, Takeshi Mizushima and James Avery Sauls for helpful discussions and comments. KM thanks Mark Alford for the kind hospitality and discussions in Washington University in St. Louis where part of this work was carried out under the support of ALPS Program, University of Tokyo. KM is supported by JSPS Research Fellowship for Young Scientists. The work of M. N. is supported in part by a Grant-in-Aid for Scientific Research on Innovative Areas “Topological Materials Science” (KAKENHI Grant No. 15H05855) and “Nuclear Matter in Neutron Stars Investigated by Experiments and Astronomical Observations” (KAKENHI Grant No. 15H00841) from the the Ministry of Education, Culture, Sports, Science (MEXT) of Japan. The work of M. N. is also supported in part by the Japan Society for the Promotion of Science (JSPS) Grant-in-Aid for Scientific Research (KAKENHI Grant No. 25400268) and by the MEXT-Supported Program for the Strategic Research Foundation at Private Universities “Topological Science” (Grant No. S1511006).

### Appendix A: Ground state with the sixth order term

In this appendix, we determine the ground state taking into account the sixth order term in the GL free energy. We correct the amplitude of the state with the sixth order term previously obtained in Ref. [15], but the difference is negligible. We also show that off-diagonal elements do not appear, and so the state remains in the nematic phase even when we take into account the sixth order term.

We consider the following free energy;

$$F = \int d^3\rho (f_4 + f_6). \quad (\text{A1})$$

By minimizing  $f_4$ , we can obtain the ground state up to

fourth order  $A_{4\text{th}}$ ,

$$A_{4\text{th}} = \sqrt{\frac{|\alpha|}{6\beta}} \begin{pmatrix} 1 & 0 & 0 \\ 0 & 1 & 0 \\ 0 & 0 & -2 \end{pmatrix}. \quad (\text{A2})$$

To see the ground state up to the sixth order, we expand the order parameter  $A$  as follows:

$$\begin{aligned} A &= A_{4\text{th}} + \Delta A \\ &= A_{4\text{th}} + i\sqrt{\frac{|\alpha|}{6\beta}} \begin{pmatrix} f_1 & g & h \\ g & f_2 & j \\ h & j & -f_1 - f_2 \end{pmatrix}. \end{aligned} \quad (\text{A3})$$

Then, we put this order parameter into the free energy density and expand it up to the second order with respect to the  $\Delta A$ :

$$\begin{aligned} F &= \int d^3\rho \left[ \frac{\alpha^2}{18\beta} ((f_1 - f_2)^2 + 4g^2 + 10h^2 + 10j^2) \right. \\ &\quad \left. + \gamma \frac{|\alpha|^3}{216\beta^3} (1704f_1^2 + 1704f_2^2 + 768f_1f_2 \right. \\ &\quad \left. + 2640g^2 + 5808h^2 + 5808j^2) \right]. \end{aligned} \quad (\text{A4})$$

Therefore, if we take  $f_1 = f_2$ , we can obtain the lower free energy density since  $\gamma$  is negative. Next, we assume that the ground state up to the sixth order to be

$$A_{6\text{th}} = N_{6\text{th}} \begin{pmatrix} 1 & 0 & 0 \\ 0 & 1 & 0 \\ 0 & 0 & -2 \end{pmatrix}. \quad (\text{A5})$$

By minimizing the free energy with respect to  $N_{6\text{th}}$ , we get

$$N_{6\text{th}} \equiv \sqrt{\frac{6\beta - \sqrt{(6\beta)^2 - 2784\alpha\gamma}}{1392|\gamma|}}. \quad (\text{A6})$$

Finally, let us expand the free energy density by using

$$\begin{aligned} A &= A_{6\text{th}} + \Delta' A \\ &= A_{6\text{th}} + iN_{6\text{th}} \begin{pmatrix} f_1 & g & h \\ g & f_2 & j \\ h & j & -f_1 - f_2 \end{pmatrix}. \end{aligned} \quad (\text{A7})$$

We thus reach at

$$F = \int d^3\rho (c_1(f_1 - f_2)^2 + c_2g^2 + c_3h^2 + c_4j^2) \quad (\text{A8})$$

where each coefficients  $c_1$ ,  $c_2$ ,  $c_3$  and  $c_4$  are positive. Therefore, we have shown that  $A_{6\text{th}}$  is at least at the local minimum.

### Appendix B: Equation of motion

In this appendix, we write down the equation of motion in the cylindrical basis ( $n = 1$ ) and  $xyz$ -basis ( $n = 0$ ).

- The equation of motions for cylindrical basis ( $n = 1$ ) are given as follows:

$$\begin{aligned}
& 7\frac{\partial^2 f_1}{\partial \rho^2} + \frac{1}{\rho} \left( 5\frac{\partial f_1}{\partial \rho} - 4\frac{\partial f_2}{\partial \rho} - 2\delta_{m,0}\frac{\partial g}{\partial \rho} \right) + \frac{1}{\rho^2} (-15f_1 + 14f_2 + 22\delta_{m,0}g) + 3f_1 \\
& - f_1 \left( f_1^2 + f_2^2 + f_1 f_2 + \frac{5 + 2\delta_{m,0}}{3} g^2 \right) + f_2 \left( \frac{1 + \delta_{m,0}}{3} g^2 \right) \\
& - \frac{|\alpha|}{36\beta^2} \gamma \left( 216f_1^5 + 408f_1^4 f_2 + 672f_1^3 f_2^2 + 528f_1^2 f_2^3 + 264f_1 f_2^4 + g^2((972 + 516\delta_{m,0})f_1^3 \right. \\
& + (504 + 120\delta_{m,0})f_1^2 f_2 + (612 + 300\delta_{m,0})f_1 f_2^2 - (216 + 168\delta_{m,0})f_2^3) + g^4((504 + 264\delta_{m,0})f_1 \\
& \left. - (144 + 168\delta_{m,0})f_2) \right) + \frac{g}{|\alpha|} \times \begin{cases} -(f_1 + f_2)H_z^2 & (\mathbf{H} \parallel \mathbf{z}) \\ f_2 H_\theta^2 & (\mathbf{H} \parallel \boldsymbol{\theta}) \end{cases} = 0, \tag{B1}
\end{aligned}$$

$$\begin{aligned}
& 3\frac{\partial^2 f_2}{\partial \rho^2} - 2\frac{\partial^2 f_1}{\partial \rho^2} + \frac{1}{\rho} \left( 2\frac{\partial f_1}{\partial \rho} + 5\frac{\partial f_2}{\partial \rho} - 2\delta_{m,0}\frac{\partial g}{\partial \rho} \right) + \frac{1}{\rho^2} (12f_1 - 19f_2 - 26\delta_{m,0}g) + 3f_2 \\
& - f_2 \left( f_1^2 + f_2^2 + f_1 f_2 + \frac{5 + 2\delta_{m,0}}{3} g^2 \right) + f_1 \left( \frac{1 + \delta_{m,0}}{3} g^2 \right) \\
& - \frac{|\alpha|}{36\beta^2} \gamma \left( 216f_2^5 + 408f_2^4 f_1 + 672f_2^3 f_1^2 + 528f_2^2 f_1^3 + 264f_2 f_1^4 + g^2((972 + 516\delta_{m,0})f_2^3 \right. \\
& + (504 + 120\delta_{m,0})f_2^2 f_1 + (612 + 300\delta_{m,0})f_2 f_1^2 - (216 + 168\delta_{m,0})f_1^3) + g^4((504 + 264\delta_{m,0})f_2 \\
& \left. - (144 + 168\delta_{m,0})f_1) \right) + \frac{g}{|\alpha|} \times \begin{cases} -(f_1 + f_2)H_z^2 & (\mathbf{H} \parallel \mathbf{z}) \\ -2f_2 H_\theta^2 & (\mathbf{H} \parallel \boldsymbol{\theta}) \end{cases} = 0, \tag{B2}
\end{aligned}$$

$$\begin{aligned}
& 2\frac{\partial^2 g}{\partial \rho^2} + \frac{1}{\rho} \left( \delta_{m,0}\frac{\partial f_1}{\partial \rho} + \delta_{m,0}\frac{\partial f_2}{\partial \rho} + 2\frac{\partial g}{\partial \rho} \right) + \frac{1}{\rho^2} (3\delta_{m,0}f_1 - 5\delta_{m,0}f_2 - (8 + 2(m+1)^2)g) + g \\
& - \frac{g}{6} ((3 + \delta_{m,0})f_1^2 + (3 + \delta_{m,0})2f_2^2 + 2f_1 f_2 + 2g^2) \\
& - \frac{|\alpha|}{36\beta^2} \gamma \left( 72g^5 + ((288 + 120\delta_{m,0})f_1^2 + (144 - 48\delta_{m,0})f_1 f_2 + (288 + 120\delta_{m,0})f_2^2)g^3 \right. \\
& + ((144 + 72\delta_{m,0})f_1^4 + (180 + 60\delta_{m,0})f_1^3 f_2 + (288 + 120\delta_{m,0})f_1^2 f_2^2 + (180 + 60\delta_{m,0})f_1 f_2^3 \\
& \left. + (144 + 72\delta_{m,0})f_2^4)g \right) + \frac{g}{|\alpha|} \times \begin{cases} 0 & (\mathbf{H} \parallel \mathbf{z}) \\ -gH_\theta^2/2 & (\mathbf{H} \parallel \boldsymbol{\theta}) \end{cases} = 0. \tag{B3}
\end{aligned}$$

- The equation of motions for  $xyz$ -basis ( $n = 0$ ) are given as follows:

$$\begin{aligned}
& 5\frac{\partial^2 f_1}{\partial \rho^2} - \frac{\partial^2 f_2}{\partial \rho^2} + \frac{1}{2}(-\delta_{m,2} + \delta_{m,-2})\frac{\partial^2 g}{\partial \rho^2} + \frac{1}{\rho} \left( 5\frac{\partial f_1}{\partial \rho} - \frac{\partial f_2}{\partial \rho} + \left( -\frac{3}{2}\delta_{m,2} - \frac{1}{2}\delta_{m,-2} \right) \frac{\partial g}{\partial \rho} \right) \\
& + \frac{1}{\rho^2} \left( -5f_1 + f_2 + \frac{1}{2}(-\delta_{m,2} + \delta_{m,-2})g \right) \\
& + 3f_1 - f_1 \left( f_1^2 + f_2^2 + f_1 f_2 + \frac{5 + 2\delta_{m,0}}{3} g^2 \right) + f_2 \left( \frac{1 + \delta_{m,0}}{3} g^2 \right) \\
& - \frac{|\alpha|}{36\beta^2} \gamma \left( 216f_1^5 + 408f_1^4 f_2 + 672f_1^3 f_2^2 + 528f_1^2 f_2^3 + 264f_1 f_2^4 + g^2((972 + 516\delta_{m,0})f_1^3 \right. \\
& + (504 + 120\delta_{m,0})f_1^2 f_2 + (612 + 300\delta_{m,0})f_1 f_2^2 - (216 + 168\delta_{m,0})f_2^3) + g^4((504 + 264\delta_{m,0})f_1 \\
& \left. - (144 + 168\delta_{m,0})f_2) \right) + \frac{g}{|\alpha|} \times \begin{cases} -(f_1 + f_2)H_z^2 & (\mathbf{H} \parallel \mathbf{z}) \\ f_2 H_\theta^2 & (\mathbf{H} \parallel \boldsymbol{\theta}) \end{cases} = 0, \tag{B4}
\end{aligned}$$

$$\begin{aligned}
& 5 \frac{\partial^2 f_2}{\partial \rho^2} - \frac{\partial^2 f_1}{\partial \rho^2} + \frac{1}{2}(-\delta_{m,2} + \delta_{m,-2}) \frac{\partial^2 g}{\partial \rho^2} + \frac{1}{\rho} \left( 5 \frac{\partial f_2}{\partial \rho} - \frac{\partial f_1}{\partial \rho} + \left( -\frac{3}{2} \delta_{m,2} - \frac{1}{2} \delta_{m,-2} \right) \frac{\partial g}{\partial \rho} \right) \\
& + \frac{1}{\rho^2} \left( -5f_2 + f_1 + \frac{1}{2}(-\delta_{m,2} + \delta_{m,-2})g \right) \\
& + 3f_2 - f_2 \left( f_1^2 + f_2^2 + f_1 f_2 + \frac{5 + 2\delta_{m,0}}{3} g^2 \right) + f_1 \left( \frac{1 + \delta_{m,0}}{3} g^2 \right) \\
& - \frac{|\alpha|}{36\beta^2} \gamma \left( 216f_2^5 + 408f_2^4 f_1 + 672f_2^3 f_1^2 + 528f_2^2 f_1^3 + 264f_2 f_1^4 + g^2((972 + 516\delta_{m,0})f_2^3 \right. \\
& + (504 + 120\delta_{m,0})f_2^2 f_1 + (612 + 300\delta_{m,0})f_2 f_1^2 - (216 + 168\delta_{m,0})f_1^3) + g^4((504 + 264\delta_{m,0})f_2 \\
& \left. - (144 + 168\delta_{m,0})f_1) \right) + \frac{g}{|\alpha|} \times \begin{cases} -(f_1 + f_2)H_z^2 & (\mathbf{H} \parallel \mathbf{z}) \\ -2f_2 H_\theta^2 & (\mathbf{H} \parallel \boldsymbol{\theta}) \end{cases} = 0, \tag{B5}
\end{aligned}$$

$$\begin{aligned}
& 2 \frac{\partial^2 g}{\partial \rho^2} + \frac{1}{4}(-\delta_{m,2} + \delta_{m,-2}) \left( \frac{\partial^2 f_1}{\partial \rho^2} + \frac{\partial^2 f_2}{\partial \rho^2} \right) + \frac{1}{\rho} \left( \left( \frac{1}{4} \delta_{m,2} + \frac{3}{4} \delta_{m,-2} \right) \left( \frac{\partial f_1}{\partial \rho} + \frac{\partial f_2}{\partial \rho} \right) + 2 \frac{\partial g}{\partial \rho} \right) \\
& + \frac{1}{\rho^2} \left( \frac{m+1}{4}(-\delta_{m,2} + \delta_{m,-2})(f_1 + f_2) - 2(m+1)^2 g \right) \\
& + g - \frac{g}{6} ((3 + \delta_{m,0})f_1^2 + (3 + \delta_{m,0})2f_2^2 + 2f_1 f_2 + 2g^2) \\
& - \frac{|\alpha|}{36\beta^2} \gamma \left( 72g^5 + ((288 + 120\delta_{m,0})f_1^2 + (144 - 48\delta_{m,0})f_1 f_2 + (288 + 120\delta_{m,0})f_2^2)g^3 \right. \\
& + ((144 + 72\delta_{m,0})f_1^4 + (180 + 60\delta_{m,0})f_1^3 f_2 + (288 + 120\delta_{m,0})f_1^2 f_2^2 + (180 + 60\delta_{m,0})f_1 f_2^3 \\
& \left. + (144 + 72\delta_{m,0})f_2^4)g \right) + \frac{g}{|\alpha|} \times \begin{cases} 0 & (\mathbf{H} \parallel \mathbf{z}) \\ -gH_\theta^2/2 & (\mathbf{H} \parallel \boldsymbol{\theta}) \end{cases} = 0. \tag{B6}
\end{aligned}$$

- 
- [1] A. B. Migdal, Nucl. Phys. **13**, 655 (1959).  
[2] P. E. Reichley and G. S. Downs, Nature **234**, 48 (1971).  
[3] G. Baym, C. J. Pethick, D. Pines, and M. Ruderman, Nature **224**, 879 (1969).  
[4] D. Pines, J. Shaham, and M. Ruderman, Nature, Phys. Sci. **237**, 83 (1972).  
[5] T. Takatsuka and R. Tamagaki, Prog. Theor. Phys. **79**, 274 (1988).  
[6] P. W. Anderson and N. Itoh, Nature **256**, 25 (1975).  
[7] C. O. Heinke and W. C. G. Ho, Astrophys. J. **719**, L167 (2010), arXiv:1007.4719 [astro-ph.HE].  
[8] D. Page, M. Prakash, J. M. Lattimer, and A. W. Steiner, Phys. Rev. Lett. **106**, 081101 (2011), arXiv:1011.6142 [astro-ph.HE].  
[9] R. Tamagaki, Prog. Theor. Phys. **44**, 905 (1970).  
[10] M. Hoffberg, A. E. Glassgold, R. W. Richardson, and M. Ruderman, Phys. Rev. Lett. **24**, 775 (1970).  
[11] T. Takatsuka and R. Tamagaki, Prog. Theor. Phys. **46**, 114 (1971).  
[12] T. Takatsuka, Prog. Theor. Phys. **47**, 1062 (1972).  
[13] T. Fujita and T. Tsuneto, Prog. Theor. Phys. **48**, 766 (1972).  
[14] R. W. Richardson, Phys. Rev. D **5**, 1883 (1972).  
[15] J. Sauls and J. Serene, Phys. Rev. D **17**, 1524 (1978).  
[16] N. D. Mermin, Phys. Rev. **A9**, 868 (1974).  
[17] V. Z. Vulovic and J. A. Sauls, Phys. Rev. **D29**, 2705 (1984).  
[18] P. Muzikar, J. A. Sauls, and J. W. Serene, Phys. Rev. D **21**, 1494 (1980).  
[19] J. A. Sauls, D. L. Stein, and J. W. Serene, Phys. Rev. D **25**, 967 (1982).  
[20] P. F. Bedaque, G. Rupak, and M. J. Savage, Phys. Rev. **C68**, 065802 (2003), arXiv:nucl-th/0305032 [nucl-th].  
[21] P. F. Bedaque and A. N. Nicholson, Phys. Rev. **C87**, 055807 (2013), [Erratum: Phys. Rev. C **89**, no. 2, 029902 (2014)], arXiv:1212.1122 [nucl-th].  
[22] P. F. Bedaque, A. N. Nicholson, and S. Sen, Phys. Rev. **C92**, 035809 (2015), arXiv:1408.5145 [nucl-th].  
[23] L. B. Leinson, Phys. Rev. **C81**, 025501 (2010), arXiv:0912.2164 [astro-ph.SR].  
[24] L. B. Leinson, Phys. Lett. **B689**, 60 (2010), arXiv:1001.2617 [astro-ph.SR].  
[25] L. B. Leinson, Phys. Rev. **C82**, 065503 (2010), [Erratum: Phys. Rev. C **84**, 049901 (2011)], arXiv:1012.5387 [hep-ph].  
[26] L. B. Leinson, Phys. Rev. **C83**, 055803 (2011), arXiv:1007.2803 [hep-ph].  
[27] L. B. Leinson, Phys. Rev. **C84**, 045501 (2011), arXiv:1110.2145 [nucl-th].  
[28] L. B. Leinson, Phys. Rev. **C85**, 065502 (2012), arXiv:1206.3648 [nucl-th].  
[29] L. B. Leinson, Phys. Rev. **C87**, 025501 (2013), arXiv:1301.5439 [nucl-th].  
[30] L. B. Leinson, Phys. Lett. **B741**, 87 (2015), arXiv:1411.6833 [astro-ph.SR].  
[31] L. B. Leinson, (2015), arXiv:1509.02827 [astro-ph.HE].

- [32] K. M. Shahabasyan and M. K. Shahabasyan, *Astrophysics* **54**, 429 (2011), [Astrofiz.54,483(2011)].
- [33] J. A. Sauls, *Anisotropic Superfluidity in Neutron Stars and Strong Coupling Effect in Superfluid  $^3\text{He}$* , Ph.D. thesis, SUNY Stony Brook (1980).
- [34] D. Vollhardt and P. Woelfle, *The Superfluid Phases Of Helium 3* (Taylor & Francis, 1990).
- [35] G. E. Volovik, *The universe in a helium droplet*, Vol. 117 (Oxford University Press, 2009).
- [36] Y. Kawaguchi and M. Ueda, *Phys. Rept.* **520**, 253 (2012).
- [37] R. Barnett, A. Turner, and E. Demler, *Phys. Rev. Lett.* **97**, 180412 (2006).
- [38] S. Uchino, M. Kobayashi, M. Nitta, and M. Ueda, *Phys. Rev. Lett.* **105**, 230406 (2010), arXiv:1010.2864 [cond-mat.quant-gas].
- [39] S. Kobayashi, M. Kobayashi, Y. Kawaguchi, M. Nitta, and M. Ueda, *Nucl. Phys.* **B856**, 577 (2012), arXiv:1110.1478 [math-ph].
- [40] J. L. Song, G. W. Semanoff, and F. Zhou, *Phys. Rev. Lett.* **98**, 160408 (2007), arXiv:cond-mat/0702052 [cond-mat.other].
- [41] In the context of spinor BEC, this is simply called as the BN phase [36, 40].
- [42] Since the boundary condition for  $g$  are zero for  $\rho = 0, \infty$  (for  $n \neq -1$ ), it is a ring-shape if it appears, and  $m$  denotes how many times the phase of  $g$  is twisted along the ring, see Ref. [53] for a similar example in a spinor BEC.
- [43] N. D. Mermin, *Rev. Mod. Phys.* **51**, 591 (1979).
- [44] M. Kobayashi, Y. Kawaguchi, M. Nitta, and M. Ueda, *Phys. Rev. Lett.* **103**, 115301 (2009), arXiv:0810.5441 [cond-mat.other].
- [45] M. Nitta, M. Shifman, and W. Vinci, *Phys. Rev.* **D87**, 081702 (2013), arXiv:1301.3544 [cond-mat.other].
- [46] M. G. Alford, A. Schmitt, K. Rajagopal, and T. Schafer, *Rev. Mod. Phys.* **80**, 1455 (2008), arXiv:0709.4635 [hep-ph].
- [47] A. P. Balachandran, S. Digal, and T. Matsuura, *Phys. Rev.* **D73**, 074009 (2006), arXiv:hep-ph/0509276 [hep-ph].
- [48] E. Nakano, M. Nitta, and T. Matsuura, *Phys. Rev.* **D78**, 045002 (2008), arXiv:0708.4096 [hep-ph].
- [49] M. Eto and M. Nitta, *Phys. Rev.* **D80**, 125007 (2009), arXiv:0907.1278 [hep-ph].
- [50] M. Eto, M. Nitta, and N. Yamamoto, *Phys. Rev. Lett.* **104**, 161601 (2010), arXiv:0912.1352 [hep-ph].
- [51] M. Eto, Y. Hirono, M. Nitta, and S. Yasui, *PTEP* **2014**, 012D01 (2014), arXiv:1308.1535 [hep-ph].
- [52] M. Cipriani, W. Vinci, and M. Nitta, *Phys. Rev.* **D86**, 121704 (2012), arXiv:1208.5704 [hep-ph].
- [53] S. Kobayashi, Y. Kawaguchi, M. Nitta, and M. Ueda, *Phys. Rev.* **A86**, 023612 (2012), arXiv:1204.0202 [cond-mat.quant-gas].